Journal of Materials Chemistry

www.rsc.org/materials

Volume 19 | Number 5 | 7 February 2009 | Pages 553–668

ISSN 0959-9428

RSC Publishing

Storage performance of $LiFePO_4$ nanoplates†

Kuppan Saravanan,[a] M. V. Reddy,[b] Palani Balaya,*[c] Hao Gong,[d] B. V. R. Chowdari[b] and Jagadese J. Vittal*[a]

Received 2nd October 2008, Accepted 30th October 2008
First published as an Advance Article on the web 8th December 2008
DOI: 10.1039/b817242k

The morphology of electrode materials is addressed as a key factor controlling rapid lithium storage in anisotropic systems such as $LiFePO_4$. In view of this, we have synthesized nanoplates of $LiFePO_4$ with a uniform coating of a 5 nm thick amorphous carbon layer by the solvothermal method and investigated their electrochemical storage behavior. The obtained nanoplates are well characterized by XRPD, SEM, HRTEM and XPS techniques. The thickness along the *b*-axis is found to be 30–40 nm; such a morphology favors short diffusion lengths for Li^+ ions, while the external conductive carbon coating provides connectivity for facile electron diffusion, resulting in high rate performances. Increase in the size of the nanoplates results in poor lithium storage performance. The storage performance of nanoplates is compared with that of mesoporous nanoparticles of $LiFePO_4$ with non-uniform carbon coating. This paper thus describes the advantages of thinner nanoplates for high rate storage performances of battery electrode materials.

Introduction

Following the report of Padhi *et al.*,[1] olivine based lithium iron phosphate, $LiFePO_4$, has attracted a lot of attention for various reasons such as ease of synthesis, low cost, it is environmentally benign, and has reduced reactivity with electrolytes resulting in very flat potential during charge/discharge processes.[2–8] Despite these advantages, the observed electrochemical performances of $LiFePO_4$ was found to be less impressive at high rates (*i.e.*, storage capacity drops significantly at high current density)[2,8] as it is a poor conductor of both electrons and Li^+ ions.[9–12] It is reported based on *ab-initio*[13] calculations as well as atomistic simulations[14] that Li^+ ions preferably move along the *b*-axis rather than along the *a*- or *c*-axes in crystals with orthorhombic space group *Pnma*. A recent report on the electronic and ionic properties of anisotropic $LiFePO_4$ single crystals by Amin *et al.*[9] further claims that the Li^+ conductivity is nearly four orders of magnitude lower than the electronic conductivity along the *b*- and *c*-axes and many orders of magnitude lower along the *a*-axis, meaning that mass transport of Li^+ is crucial for improving the kinetic issues. In this context, in order to achieve optimal storage performance preferably at high rates, it is mandatory to reduce the crystallite size along the *b*-axis for rapid extraction of both Li^+ ions and electrons from the bulk. Also exterior decoration by conductive materials such as carbon to enhance the electronic wiring among neighboring particles has been suggested.[15–18]

It is the intention of this contribution to establish such a morphology of $LiFePO_4$ crystallites with short *b*-axis and thin surface coating using conductive carbon, to improve its rate performance. Hu *et al.*[8] have shown high rate performance in $LiFePO_4$ with a discontinuous coating of carbon by filling the gap using RuO_2. However, RuO_2 is quite expensive for practical applications. Here we present a simple and inexpensive synthesis using a solvothermal method to reduce the *b*-axis to the smallest possible thickness reported so far,[19–21] with a uniform coating of carbon on the surface to achieve such high rate performances.

Various synthetic routes, such as sol–gel,[22] hydrothermal,[21,23] carbothermal,[24] co-precipitation,[25] freeze-drying,[26] template mediated approach,[27] ballmilling followed by solid state reactions[28] and microwave hydrothermal method,[29] have been adopted to synthesize $LiFePO_4$. Though some reports on $LiFePO_4$ nanoplates are available, they have not been systematically investigated especially in terms of the effect of *b*-axis thickness on the electrochemical properties of $LiFePO_4$. In this work the thickness of the synthesized nanoplates was varied by changing the reaction conditions, and its influence on the electrochemical performance was evaluated.

Experimental

Synthesis

Carbon coated thin nanoplates of $LiFePO_4$ were synthesized using a solvothermal method. A stoichiometric mixture of starting materials lithium dihydrogen phosphate (LiH_2PO_4, Aldrich), iron(II) oxalate dihydrate ($FeC_2O_4 \cdot 2H_2O$, Merck) and D-gluconic acid lactone ($C_6H_{10}O_6$, Aldrich) in the molar ratio of 1:1:5 were placed in a Teflon vessel, 25 ml of ethylene glycol (EG) was added and the vessel was sealed tightly in a stainless-steel autoclave. The autoclave was heated to 250 °C for 8 h in an oven, and then it was allowed to cool to ambient temperature. The black precipitates obtained were washed several times with ethanol and dried. Here D-gluconic acid lactone acts as the carbon source resulting in a uniform carbon coating on $LiFePO_4$ particles. Similarly carbon coated thick nanoplates of $LiFePO_4$ were synthesized using the same method except the temperature

[a]*Department of Chemistry, National University of Singapore (NUS), Singapore 117543. E-mail: chmjjv@nus.edu.sg*
[b]*Department of Physics, NUS, Singapore 117542*
[c]*Department of Mechanical Engineering, NUS, Singapore 119260. E-mail: mpepb@nus.edu.sg*
[d]*Department of Materials Science and Engineering, NUS, Singapore 119260*

† Electronic supplementary information (ESI) available: X-ray powder patterns and FESEM images. See DOI: 10.1039/b817242k

(315 °C) and time (24 h) of the reaction were altered. As-synthesized $LiFePO_4$/C was annealed at 400 °C for 4 h in an Ar–H_2 (95:5) atmosphere in order to carbonize the gluconic acid lactone completely and to increase the crystallinity of the $LiFePO_4$ samples.

Structural and electrochemical characterization

X-Ray powder diffraction (XRPD) patterns were obtained using a D5005 Bruker X-ray diffractometer equipped with Cu-Kα radiation. The accelerating voltage and current were 40 kV and 40 mA, respectively. The scan speed of 0.015° per second was used. Lattice parameters were obtained using TOPAS-R (version 2.1) software. Scanning electron microscopy (SEM) images were taken with a Jeol JSM-6700F field emission scanning electron microscope (FESEM) operated at 5 kV and 10 mA. For SEM analysis the samples were coated with a 100 nm thin platinum coating using DC sputtering. A JEOL JEM-2010 instrument was used to get the high resolution transmission electron microscopy (HRTEM) images to study the morphology and measure the carbon layer thickness of the $LiFePO_4$/C nanoplates. X-Ray photoelectron spectra of the compounds were obtained using a VG Scientific ESCA MK II spectrometer with monochromatic Mg-Kα radiation (1253.6 eV) in the range 0–1099 eV (constant-pass energy = 50 eV) and the high resolution spectra were recorded in a constant pass energy mode (20 eV). Charge referencing was carried out against adventitious carbon C, (C 1s binding energy = 284.6 eV). Analysis of the XPS spectra was done using XPS Peak-fit software. A Shirley-type background was subtracted from the recorded spectra and curve fitting was carried out with a Gaussian–Lorentzian (ratio 60:40) curve. The derived binding energies (BE) are accurate to ±0.1 eV.

For electrochemical studies, composite electrodes were fabricated with the active material, super P carbon black and binder (Kynar 2801) in the weight ratio 70:15:15 using *N*-methylpyrrolidone (NMP) as solvent. Electrodes with thickness of 10 μm were prepared using an etched aluminium foil as current collector by using the doctor-blade technique. Lithium metal foil, 1M $LiPF_6$ in ethylene carbonate (EC)–diethyl carbonate (DEC) (1:1 V/V) (Merck) and Celgard 2502 membrane were used as counter electrode, electrolyte and separator respectively to assemble coin-type cells (size 2016) in an Ar-filled glove box (MBraun, Germany). The geometrical area of the electrode was 2.0 cm^2. Details of cell fabrication have been described previously.[30] The cells were aged for 12 h before the measurements. Charge/discharge cycling at constant current mode was carried out using a computer controlled Arbin battery tester (Model, BT2000, USA) and cyclic voltammetry studies were carried out at room temperature using a computer controlled Mac-pile II system (Bio-logic, France).

Results and discussion

The XRPD pattern of the thin nanoplates is shown in Fig. 1. The XRPD pattern clearly shows single phase formation of $LiFePO_4$. As can be seen from Fig. 1 the intensities of (101), (111/201), (211/020) and (311) peaks are almost constant, whereas for the thick plates a monotonic increase of peak intensities for (101) to (311) was observed (Fig. S1†). All the peaks in the XRPD pattern

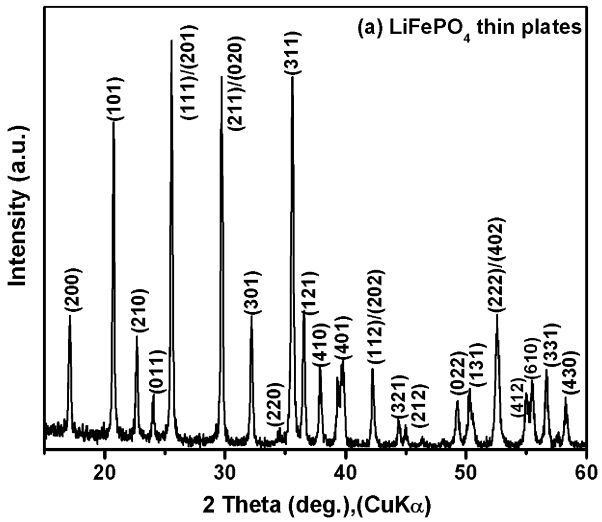

Fig. 1 XRPD pattern of the thin $LiFePO_4$/C nanoplates.

were indexed to an orthorhombic space group (JCPDS Card No: 83-2092). Obtained lattice parameters for this thin $LiFePO_4$/C plates are $a = 10.3317$ Å, $b = 6.0083$ Å and $c = 4.6946$ Å; while values of $a = 10.3311$ Å, $b = 6.0069$ Å and $c = 4.6930$ Å were found for the thick plates. These values compare well with those reported in the literature.[31]

X-Ray photoelectron spectroscopy is a non-destructive technique well-suited for the evaluation of valence states of metal/non-metal ions and extensively used in the characterization of cathode materials.[32–34] The core level spectra for Li 1s, Fe 2p, P 2p and O 1s for $LiFePO_4$/C are shown in Fig. 2a–d and the corresponding binding energies (BE) for Li 1s: 55.58 eV, Fe 2p: 710.60 ($2p_{3/2}$) and 724.3 ($2p_{1/2}$), P 2p: 133.46 eV and O 1s: 531.36 eV have been observed.

The Li 1s peak in the compound (Fig. 2a) shows a BE of 55.58 eV, which is in good agreement with values reported for $LiFePO_4$[33,34] and layered cathode materials.[32] The XPS spectrum of Fe $2p_{3/2}$ in Fig. 2b shows a BE of 710.6 (±0.2) eV which matches well with the BE of Fe^{2+} in $LiFePO_4$.[33,34] Due to the multiple splitting of the energy levels Fe ion gives rise to satellite

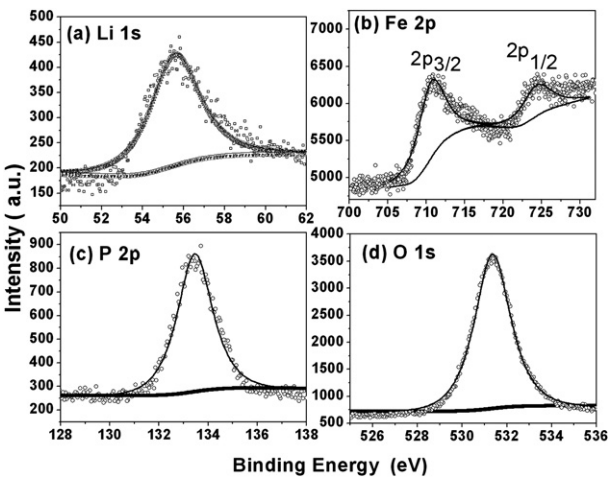

Fig. 2 XPS spectra of the $LiFePO_4$/C thin nanoplates.

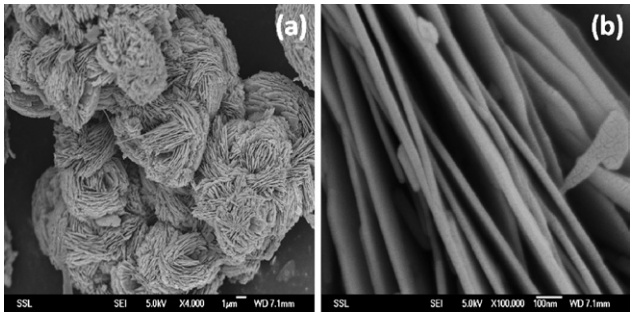

Fig. 3 FESEM images of the $LiFePO_4$/C thin nanoplates at two different magnifications.

peaks around 727.29 eV. The P 2p peak (Fig. 2c) shows a BE of 133.46 (±0.1) eV which is characteristic of the tetrahedral PO_4 group.[33,34] The single peak (Fig. 2d) for O 1s with a BE of 531.36 eV can be assigned to oxygen predominantly bonded to Fe ions in the lattice. The BE values observed here compare well with the literature.[33,34]

The FESEM images of $LiFePO_4$/C thin nanoplates are shown in Fig. 3. A lower magnification image of elliptical spheres of $LiFePO_4$/C nanoplates aligned in a parallel fashion is shown in Fig. 3a. The length of the nanoplates was not uniform and they are in the range of 4–6 μm. The width of the plates is quite difficult to measure due to the parallel alignments of the plates. When zoomed in further as shown in Fig. 3b, it is observed that the thickness of the $LiFePO_4$/C plates is in the range of 30–40 nm (averaged over 30 crystallites). It appears that EG acts as a soft template in directing the growth of nanoparticles to nanoplates at the early stages through forming hydrogen bonds, and these nanoplates further aligned tightly to form flower-like hierarchical structures[35] as shown in Fig. 3a.

The FESEM images of thick $LiFePO_4$ nanoplates are presented in Fig. 4. Higher reaction temperature (315 °C) and longer reaction time (24 h) had an impact on the plate thickness. Fig. S1† shows the XRPD pattern of the plates formed at higher temperatures. The length, width and the thickness of these plates are respectively in the range of 400–500 nm, 190 ± 10 nm and 100 ± 5 nm.

Higher temperature and longer reaction time provoke the adjacent thin plates to combine to form thicker plates along the *b*-axis while breakage of crystals in the *ac* plane resulted in a reduction of size in the other two dimensions. Solvent has

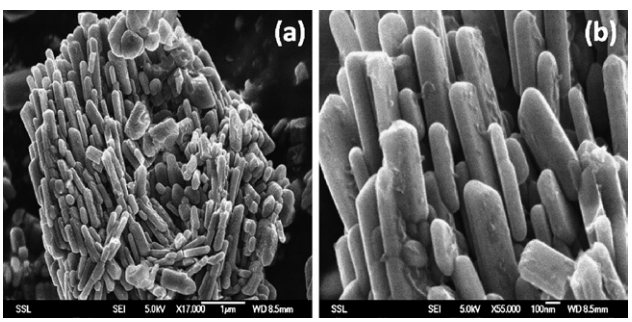

Fig. 4 FESEM images of the $LiFePO_4$/C thick nanoplates at two different magnifications.

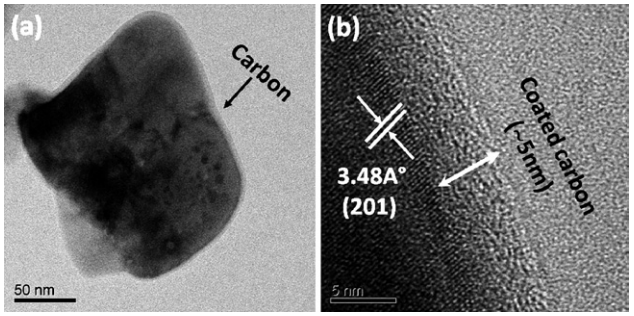

Fig. 5 TEM and high resolution TEM image of the $LiFePO_4$/C thin nanoplates. (a) TEM image showing a uniform coverage of amorphous carbon coating around the surface of a $LiFePO_4$/C nanoplate, (b) HRTEM image showing nearly 5 nm thick amorphous carbon layer around the surface of $LiFePO_4$/C.

a crucial role to play in the morphology of $LiFePO_4$: when the solvent is changed from EG to water only microrods are obtained (Fig. S2†). This clearly indicates the importance of EG in the formation of $LiFePO_4$ nanoplates and its role in self-assembly. Hydrogen bonding between the hydroxyl groups in EG allows it to exist in the long chain form.[36,37] Cations in the reaction mixture may be trapped in the network of hydrogen bonds which assist nucleation and control the crystal growth of $LiFePO_4$.

The TEM image of $LiFePO_4$/C thin nanoplates in Fig. 5a shows a uniform carbon coating with ~5 nm thickness on the surfaces of $LiFePO_4$ nanoplates. The HRTEM image (Fig. 5b) exhibits clear lattice fringes indicating single crystallinity of the nanoplates. The width (3.48 Å) of neighboring lattice fringes corresponds to the (201) plane of $LiFePO_4$.

Fig. 6a and b are the TEM image and SAED of $LiFePO_4$ nanoplates respectively. The SAED pattern viewed along [010], similar to that reported by Chen *et al.*,[19] reveals that the plate is a single crystal with the *b*-axis along the thinnest direction. The c^*/a^* ratio is found to be 2.20 from the SAED, and identical to the a/c ratio of a $LiFePO_4$ crystal with $a = 10.334$ Å, $b = 6.002$ Å and $c = 4.695$ Å. The large face of the plate (Fig. 2d) lies in the *ac* plane, viewed along the *b* direction. It is found that the thickness along *a* and *c* axes is in the range 500–800 nm, and 30–40 nm along the *b*-axis.

Voltage versus capacity plots (charge–discharge cycling) of $LiFePO_4$/C thin and thick nanoplates versus Li metal up to 50 cycles are shown in Fig. 7a and b at a current density of 17 mAg^{-1}

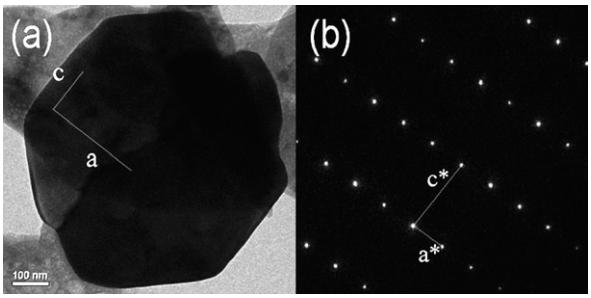

Fig. 6 (a) TEM image of the $LiFePO_4$/C plate with the *a* and *c* directions indicated, and (b) the SAED pattern of the nanoplate.

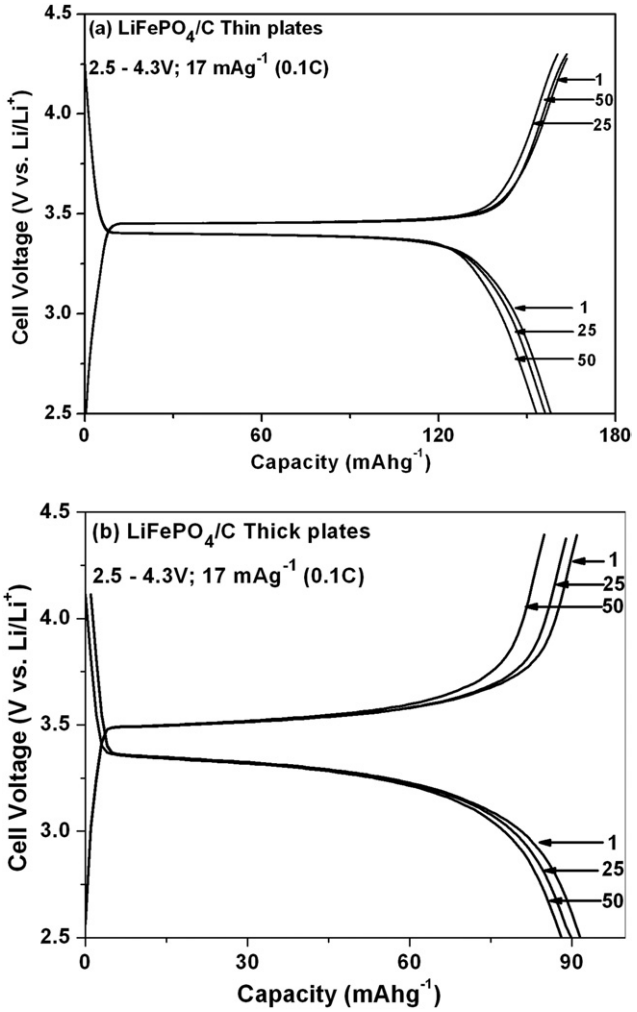

Fig. 7 Galvanostatic charge–discharge cycle curves for $LiFePO_4$/C (a) thin and (b) thick nanoplates. Current density of 17 mAg^{-1} (1C refers to a capacity of 170 mAg^{-1} in one h), potential window 2.5–4.3V, recorded at room temperature.

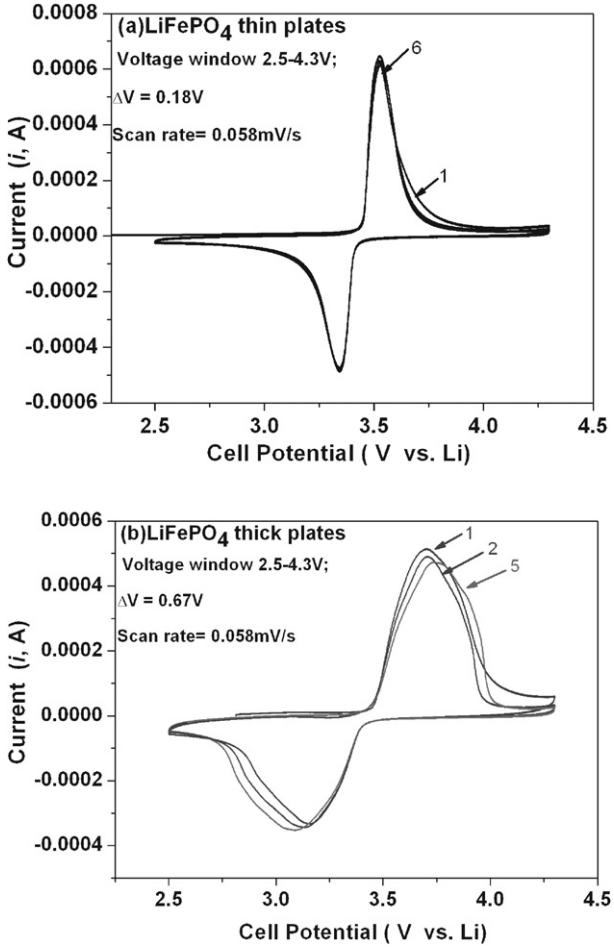

Fig. 8 Cyclic voltammograms of $LiFePO_4$/C. (a) Thin, (b) thick nanoplates. Scan rate: 0.058 mV/sec.

(0.1 C rate) in the voltage range 2.5–4.3 V. During the first charging (Li-deintercalation) process, the voltage increased sharply to ~3.45 V from the open circuit voltage (OCV = 3.0 V) followed by a long plateau till about 125 $mAhg^{-1}$ (Fig. 7a) and then gradually increased to the cut-off voltage value resulting in a storage capacity of 165 $mAhg^{-1}$ (which is close to the theoretical value of 170 $mAhg^{-1}$). The discharge curve shows a similar plateau region. The irreversible capacity loss between the first charge and discharge reactions is only ~10 $mAhg^{-1}$. Much less polarization of about 60 mV (ΔV) between charging and discharging plateaus (at 0.5 mol Li^+ insertion) was observed (Fig. 7a).

In order to ascertain the influence of the thickness of the $LiFePO_4$/C nanoplates, we studied the charge–discharge cycling of the thicker plates and the plots are shown in Fig. 7b. The thicker plates show higher polarization of about 210 mV (ΔV) (at 0.5 mol Li^+ insertion) between two plateaus (Fig. 7b). The electrochemical performance of the thicker nanoplates of $LiFePO_4$ was found to be less than 95 $mAhg^{-1}$ at a rate of 0.1 C over the voltage window 2.5–4.3 V.

The cyclic voltammograms (CV) of thin and thick nanoplates of $LiFePO_4$/C are shown in Fig. 8a and b respectively. The CV was recorded with Li metal as the counter and reference electrodes in the voltage range of 2.5–4.3 V at the scan rate of 0.058 mVs^{-1} up to 6 cycles at room temperature. The major anodic/cathodic peaks just below 3.67 V are assigned to the $Fe^{2+/3+}$ redox couple/structural transformations.[26] During the first cycle (*i.e.*, Li-deintercalation), the anodic peak is at 3.66 V (versus Li) whereas the corresponding cathodic peak is at 3.31 V. In the second cycle, the anodic peak and the corresponding cathodic peak are unaltered; this infers good reversibility of $LiFePO_4$/C thin nanoplates. The hysteresis (ΔV = the difference between the 5^{th} anodic and cathodic peak voltages) for thin nanoplates was 0.18 V whereas a huge hysteresis (ΔV) of 0.67 V was observed for the thick plates similar to the hysteresis shown in galvanostatic cycling of thin and thick plates (Fig. 7).

These results reiterate the importance of reducing the thickness along the *b*-axis to maximize facile insertion/extraction of Li^+ ions. Thin plates (30–40 nm along the *b*-axis) of $LiFePO_4$ exhibit excellent storage performance with reduced polarization. On the other hand, the rate performance observed for the 100 ± 5 nm nanoplates was found to be lower than that observed for other nanoplates of similar size reported in the literature.[21] Since the experimental conditions employed to prepare the nanoplates are

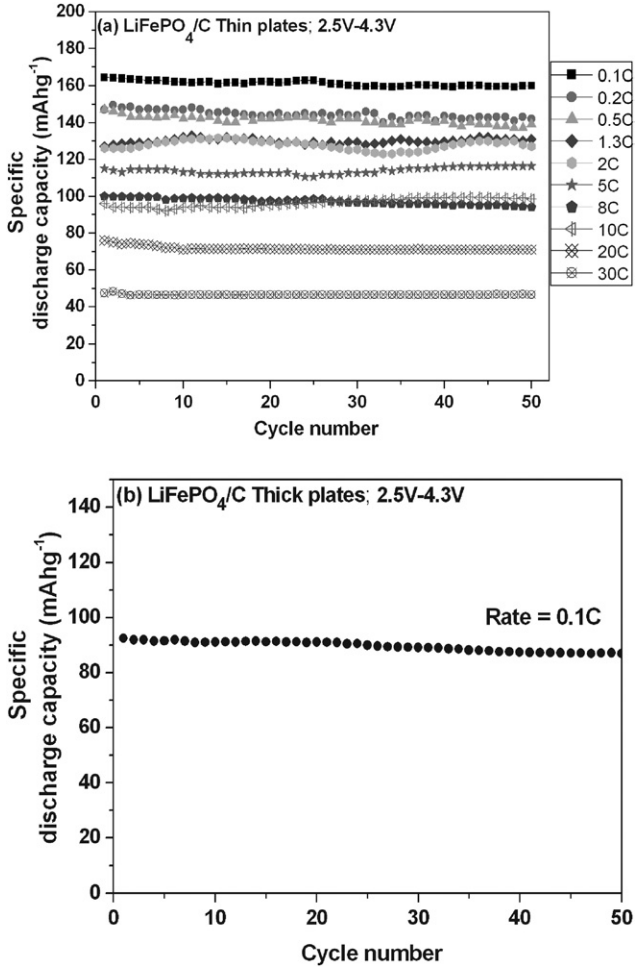

Fig. 9 Capacity vs. cycle number plots of $LiFePO_4$/C nanoplates: (a) thin plates at various current rates 0.1 to 30 C and (b) thick plates at 0.1 C rate.

different, it is not surprising to have such differences in the performances.

The specific discharge capacities versus cycle number at various current rates for thin and thick $LiFePO_4$/C nanoplates are shown in Fig. 9. It can be seen from Fig. 9a that at the end of the 10th cycle the reversible capacities are 165 ($\pm$3) $mAhg^{-1}$ at 0.1 C rate (17 mAg^{-1}) and $\sim$50 ($\pm$3) $mAhg^{-1}$ at 30 C rate (5100 mAg^{-1}), whereas thick nanoplates deliver 90 $mAhg^{-1}$ capacity at the end of the 25th cycle and 87 $mAhg^{-1}$ at the end of the 50th cycle (Fig. 9b). The above results thus clearly demonstrates the effects of nanoplate thickness on electrochemical performance. The electrochemical performance of the thin nanoplates at 0.1 C rate (17 mAg^{-1}) during the 40th cycle is much better than that of those those synthesized by the hydrothermal method.[21]

While the storage performance at high rates is better than those of mesoporous spherical $LiFePO_4$/C electrode materials with non-uniform carbon coating synthesized by the sol–gel method, it is quite comparable to the results of $LiFePO_4$ coated with carbon as well as RuO_2 layers.[8] It is worth mentioning that the present approach using solvothermal synthesis allows us to avoid the use of expensive RuO_2 coatings to achieve high rate performance of $LiFePO_4$/C electrode materials. These results emphasize the need for optimizing the morphology and hence controlling the thickness of the *b*-axis along which Li^+ diffuses.

Conclusions

In conclusion, $LiFePO_4$ nanoplates have been synthesized with a uniform coating of 5 nm thick amorphous carbon layer by a solvothermal method. The thickness along the *b*-axis is found to be 30–40 nm, and such morphology favors a shorter diffusion length for Li^+ ions, while the exterior conductive carbon decoration provides connectivity for facile electron diffusion, resulting in high rate performances. Increasing the size of the nanoplates results in poor lithium storage performance. Controlling the morphology of the electrode materials thus improves the storage performance of lithium batteries at high current operation.

Acknowledgements

We thank the Ministry of Education, Singapore for funding through NUS FRC Grant No. R143-000-283-112 and FRC Grant No. R265-000-274-133. The authors also thank Prof. G.V. Subba Rao and Dr Nagarathinam Mangayarkarasi, NUS for their valuable comments, and Dr Sudip Batabyal, Department of Chemistry, NUS for help in SEM analysis. Saravanan would like to thank NUS for the NUSNNI Graduate Scholarship.

References

1 A. K. Padhi, K. S. Nanjundaswamy and J. B. Goodenough, *J. Electrochem. Soc.*, 1997, **144**, 1188.
2 A. S. Andersson and J. O. Thomas, *J. Power. Sources*, 2001, **97–98**, 498.
3 S.-Y. Chung, J.-T. Blocking and Y.-M. Ching, *Nature Mater.*, 2002, **1**, 123.
4 N. Ravet, A. Abouimrane and M. Armand, *Nature Mater.*, 2003, **2**, 702.
5 G. Rousse, J. R- Carvajal, S. Patoux and C. Masquelier, *Chem. Mater.*, 2003, **15**, 4082.
6 (*a*) P. S. Herle, B. Ellis, N. Coombs and L. F. Nazar, *Nature Mater.*, 2004, **3**, 147; (*b*) B. Ellis, W. H. Kan, W. R. M. Makahnouk and L. F. Nazar, *J. Mater. Chem.*, 2007, **17**, 3248; (*c*) H. Fong, L. Li, Y. Yang, G. Yan and G. Li, *Chem. Commun.*, 2008, 1118.
7 A. Yamada, H. Koizumi, S.-I. Nishimura, N. Sonoyama, R. Kanno, M. Yonemura, T. Nakamura and Y. Kobayashi, *Nature Mater*, 2006, **5**, 357.
8 Y.-S. Hu, Y.-G. Guo, R. Dominko, M. Gaberscek, J. Jamnik and J. Maier, *Adv. Mater.*, 2007, **19**, 1963, and references cited therein.
9 R. Amin, P. Balaya and J. Maier, *Electrochem. Solid-State Lett.*, 2007, **10**, A13.
10 C. Delacourt, L. Laffont, R. Bouchet, C. Wurm, J.-B. Leriche, M. Morcrette, J.-M. Tarascon and C. Masquelier, *J. Electrochem. Soc.*, 2005, **152**, A913.
11 W. Ojczyk, J. Marzec, K. Świerczek, W. Zajac, M. Molenda, R. Dziembaj and J. Molenda, *J. Power Sources.*, 2007, **173**, 700.
12 D. Morgan, A. Van der Ven and G. Ceder, *Electrochem. Solid-State Lett.*, 2004, **7**, A30–A32.
13 T. Maxisch, F. Zhou and G. Ceder, *Physical review B.*, 2006, **73**, 104301.
14 M. S. Islam, D. J. Driscoll, C. A. J. Fisher and P. R. Slater, *Chem. Mater.*, 2005, **17**, 5085.
15 H. Huang, S. C. Yin and L. F. Nazar, *Electrochem. Solid-State Lett.*, 2001, **4**, A170.
16 Z. Chen and J. R. Dahn, *J. Electrochem. Soc.*, 2002, **149**, A1184.
17 J. Moskon, R. Dominko, R. C. Korosec, M. Gaberscek and J. Jamnik, *J. Power. Sources.*, 2007, **174**, 683.
18 A. Ait Salah, A. Mauger, K. Zaghib, J. B. Goodenough, N. Ravet, M. Gauthier, F. Gendron and C. M. Julien, *J. Electrochem. Soc.*, 2006, **153**, A1692.

19 G. Chen, X. Song and T. J. Richardson, *Electrochem & Solid-State Lett.*, 2006, **9**, A295.
20 L. Laffont, C. Delacourt, P. Gibot, M. Yue Wu, P. Kooyman, C. Masquelier and J. M. Tarascon, *Chem. Mater.*, 2006, **18**, 5520.
21 K. Dokko, S. Koizumi, H. Nakano and K. Kanamura, *J. Mater. Chem.*, 2007, **17**, 4803.
22 (*a*) R. Dominko, M. Bele, M. Gaberscek, M. Remskar, D. Hanzel, J. M. Goupil, S. Pejovnik and J. Jamnik, *J. Power Sources.*, 2006, **153**, 274; (*b*) M. Gaberscek, R. Dominko, M. Bele, M. Remskar, D. Hanzel and J. Jamnik, *Solid State Ionics.*, 2005, **176**, 1801.
23 S. Yang, P. Y. Zavaliji and M. S. Whittingham, *Electrochem. Commun.*, 2001, **3**, 505.
24 J. Barker, M. Y. Saidi and J. L. Swoyer, *Electrochem & Solid-State Lett.*, 2003, **6**, A53.
25 (*a*) C. Delacourt, P. Poizot, S. Levasseur and C. Masquelier, *Electrochem & Solid-State Lett.*, 2006, **9**, A352; (*b*) G. Arnold, J. Garche, R. Hemmer, S. Strobele, C. Vogler and M. W. Mehrens, *J. Power Sources*, 2003, **119–121**, 247.
26 V. Palomares, A. Goni, I. G. D. Muro, I. D. Meatza, M. Bengoechea, O. Miguel and T. Rojo, *J. Power Sources.*, 2007, **171**, 879.
27 C. R. Sides, F. Croce, V. Y. Young, C. R. Martin and B. Scrosati, *Electrochem & Solid-State Lett.*, 2005, **8**, A484.
28 C. Delmas, M. Maccario, L. Crogunnec, F. L. Cras and F. Weill, *Nature Mater.*, 2008, **7**, 655.
29 A. V Murugan, T. Muraliganth and A. Manthiram, *Electrochem. Commun*, 2008, **10**, 903.
30 M. V. Reddy, G. V. Subba Rao and B. V. R. Chowdari, *J. Phys. Chem. C.*, 2007, **111**, 11712.
31 S.-T. Myung, S. Komaba, N. Hirosaki, H. Yashiro and N. Kumagai, *Electrochem. Acta*, 2004, **49**, 4213.
32 K. S. Tan, M. V. Reddy, G. V. Subba Rao and B. V. R. Chowdari, *J. Power. Sources.*, 2005, **141**, 129.
33 Y. H. Rho, L. F. Nazar, L. Perry and D. Ryan, *J. Electrochem. Soc.*, 2007, **154**, A283.
34 A. Caballero, M. Cruz-Yusta, J. Morales, J. Santos-Pena and E. Rodriguez-Castellon, *Eur. J. Inorg. Chem.*, 2006, **2006**, 1758.
35 Y. Wang, Y. Jiang and Y. Xia, *J. Am. Chem. Soc*, 2003, **125**, 16176.
36 J. Chen, T. Herricks, M. Geissler and Y. N. Xia, *J. Am. Chem. Soc.*, 2004, **126**, 10854.
37 D. B. Yu, X. Q. Sun, J. W. Zou, Z. R. Wang, F. Wang and K. Tang, *J. Phys. Chem. B*, 2006, **110**, 21667.

